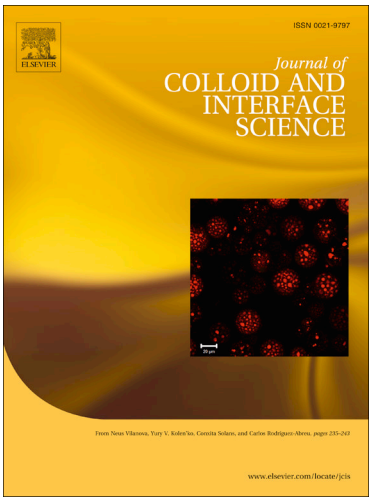

Rational Design of a Stable Peroxidase Mimic for Colorimetric Detection of H_2O_2 and Glucose: A Synergistic CeO_2/Zeolite Y Nanocomposite

Xiaowei Cheng, Le Huang, Xuanyu Yang, Ahmed A. Elzatahry, Abdulaziz Alghamdi, Yonghui Deng

PII: S0021-9797(18)31185-8
DOI: https://doi.org/10.1016/j.jcis.2018.09.101
Reference: YJCIS 24152

To appear in: *Journal of Colloid and Interface Science*

Received Date: 26 August 2018
Revised Date: 28 September 2018
Accepted Date: 28 September 2018

Please cite this article as: X. Cheng, L. Huang, X. Yang, A.A. Elzatahry, A. Alghamdi, Y. Deng, Rational Design of a Stable Peroxidase Mimic for Colorimetric Detection of H_2O_2 and Glucose: A Synergistic CeO_2/Zeolite Y Nanocomposite, *Journal of Colloid and Interface Science* (2018), doi: https://doi.org/10.1016/j.jcis.2018.09.101

Rational Design of a Stable Peroxidase Mimic for Colorimetric Detection of H_2O_2 and Glucose: A Synergistic CeO_2/Zeolite Y Nanocomposite

Xiaowei Cheng,[1,*] Le Huang,[2] Xuanyu Yang,[1]

Ahmed A. Elzatahry,[3,*] Abdulaziz Alghamdi,[4] and Yonghui Deng[1]

[1] Department of Chemistry, State Key Laboratory of Molecular Engineering of Polymers, Shanghai Key Laboratory of Molecular Catalysis and Innovative Materials, iChEM (Collaborative Innovation Center of Chemistry for Energy Materials), Fudan University, Shanghai 200433, China.

[2] School of Environmental and Chemical Engineering, Shanghai University, Shanghai 200444, China.

[3] Materials Science and Technology Program, College of Arts and Sciences, Qatar University, P.O. Box 2713, Doha, Qatar.

[4] Department of Chemistry, College of Science, King Saud University, Riyadh 11451, Saudi Arabia.

*Corresponding Author: xwcheng@fudan.edu.cn (X. W. Cheng), aelzatahry@qu.edu.qa (A. A. Elzatahry).

Abstract Owing to the high costs and instability of natural enzymes, the development of enzyme mimics based on inorganic nanomaterials has attracted a wide concern in recent years. In this work, a stable nanocomposite composed of highly dispersed CeO_2 nanoparticles decorated on zeolite Y as support (CeO_2/Y) was synthesized by a facile wet impregnation method, and the CeO_2/Y nanocomposite was firstly proposed as an efficient peroxidase-mimicking nanozyme for accurate detection of H_2O_2 and glucose. The best catalyst was the nanocomposite with CeO_2 to zeolite Y mass ratio of 0.20 (denoted as 20CeO_2/Y), showing a better affinity and higher catalytic constant to the substrate of H_2O_2 and 3,3′,5,5′-tetramethylbenzidine (TMB) than horseradish peroxidase (HRP) enzymes by the steady-state kinetic analysis. The enzyme-mimicking catalyst could be used over a wider range of pH and temperature

for a long-time reuse in TMB oxidation. A facile colorimetric assay was set up for the accurate detection of H_2O_2 and glucose, with the detection limits of 0.323 μM and 35.4 μM, respectively. The CeO_2/Y-based peroxidase mimic was used to precisely detect the glucose concentration in real blood serum samples, exhibiting a great potential to be constructed as a reliable biosensor for glucose detection in some complex systems. The superior peroxidase-mimicking performance of CeO_2/Y nanocomposite is attributed to the synergistic effects of outstanding activity of highly dispersed CeO_2 nanoparticles (5-10 nm) and adsorption properties of zeolite Y with large surface area (517 $m^2 \cdot g^{-1}$) and pore volume (0.329 $cm^3 \cdot g^{-1}$).

Keywords CeO_2/Y nanocomposite, peroxidase mimic, H_2O_2, glucose detection, colorimetric, nanozyme

1. Introduction

As the important natural biocatalysts, enzymes are involved in nearly all reactions of living organisms, which synergistically dominate the metabolism, nutrition and energy conversion, etc. On account of their unique and efficient catalytic performance, enzymes are extensively applied in food processing, chemical production, disease diagnosis, clinical therapy and many other fields [1-4]. Even so, enzymes still suffer some unavoidable drawbacks, such as high costs in separation and purification, limited operational conditions, weak storage stability to environmental changes, which largely cause difficulties for their practical applications especially in some catalytic reactions [5,6]. In recent several years, enzyme mimics or artificial nanozymes based on inorganic nanomaterials have attracted great concerns, showing the possibilities to overcome these subsistent problems of natural enzymes [7-9] and the excellent stability and activity even under severe reaction conditions [10,11]. In addition, nanomaterials possess some advantages as facile preparation in low cost and diversity in structure and composition. Therefore, considerable efforts have been devoted to developing various inorganic nanomaterials as peroxidase mimics [12-15]. Noble metal nanoparticles or nanocomposites, such as Pt nanotubes [14], Au

nanoclusters [16,17], Au-Pd bimetallic nanoparticles-graphene hybrids [18], etc, have been extensively exploited as the peroxidase-like catalysts. However, the high costs and easy inactivation of noble metals and graphene supports also limit their applications. The common low-cost metal oxides with different nanostructures, such as Fe_3O_4 nanoparticles [19], CuO nanoclusters [20], V_2O_5 nanowires [21], etc, and some other nanomaterials such as graphene nanocomposites [22], functionalized nano-MoS_2 [5], and carbon dots [23], etc, have attracted more and more attention of researchers, because they show the comparable catalytic activity with noble metals as peroxidase mimics. Nevertheless, these nanomaterials are always chemically unstable with slow deactivation under severe conditions, due to their partial etching or aggregation during the peroxidase-like catalytic reaction [24]. Thus, the chemically stable and environment friendly artificial nanozymes are imperatively desired as the mimics in bioassays and disease diagnosis [25].

To our best knowledge, composite nanomaterials with well-designed structures and mutil-functionality, such as graphene supported Au-Pd bimetallic nanoparticles [18], nanohybrids of hemin and gold nanoparticles in graphene-mesoporous silica [22], PtPd-Fe_3O_4 nanoparticles [26], etc, could achieve the enhanced catalytic performance and stability toward enzyme mimicry owing to their appropriate combination of intrinsic properties of each component. Generally, these hybrid functional materials are composed of uniformly dispersed nanoparticles and a proper matrix, which can make their peroxidase-like performance quite different from any one of the pure components [18,22,25,26]. In recent years, nanoceria (CeO_2) has attracted considerable interests as one of the most promising candidates widely used in the fields of photocatalyst [27], cytochrome accelerant [28], antioxidants [29], superoxide scavenger [30], etc. All these applications originate from the intrinsic properties of CeO_2, such as the presence of rich oxygen vacancies within crystal defects and the unique ability of reversible valence state switching between Ce^{4+} and Ce^{3+} [31-34]. Moreover, CeO_2 possesses ideal biocompatibility and redox couple similar with natural enzymes, so it could be used as a highly active enzyme mimic [33,34]. CeO_2 was reported to show strong peroxidase-like activity to some colorimetric substrates

such as TMB (3,3′,5,5′-tetramethylbenzidine), OPD (orthophenylene diamine) and ABTS (2,2′-azino-bis(3-ethylbenzothiazoline-6-sulfonic acid) diammonium salt) for H_2O_2 detection [35]. However, CeO_2 nanoparticles with high surface free energy and rich defects are quite easy to randomly agglomerate into bulky ones, showing weak catalytic activity after recycled utilization [31-36]. Therefore, in order to prevent CeO_2 nanoparticles from agglomerating as well as to promote the peroxidase-like catalytic activity and stability, it is imperative to rationally design the CeO_2/support hybrid nanocomposites through uniformly decorating CeO_2 nanoparticles on an appropriate support, such as TiO_2 nanotube [37], montmorillonite [38], etc.

Zeolites are the typical crystalline microporous aluminosilicate materials with high structural stability and controllable surface acidity, widely used as heterogeneous catalysts or catalyst supports in large-scale industrial applications [39]. Among numerous zeolites with different topologies, zeolite Y (FAU type), with 12-member-ring channels and pore size of 0.74 nm, is one of the most important aluminosilicate zeolites applied in the fields of catalysis and adsorption [40]. Zeolite Y has some intrinsic structural properties, such as hydrophilic interface, large specific surface area, huge cavity, high cation exchange capacity, and it can be produced in low cost. Therefore, zeolite Y is always utilized as an appropriate substrate for uniformly loading metal or metal oxide nanoparticles in its cages or on its surface. NaY zeolite was reported as a platform for preparation of Ag nanoparticles arrays, which can be used as an electrochemical sensor for catalytic reduction of H_2O_2 [41]. But until now, there have not been any reports about the enzyme mimics using metal oxide/zeolite hybrid nanocomposites as peroxidase-like catalysts. Herein, through a facile wet impregnation method, CeO_2/Y hybrid nanocomposites with different mass ratios were obtained by uniformly decorating CeO_2 nanoparticles on commercial zeolite Y as support. The nanocomposites were then established as a peroxidase-like catalyst in oxidation of TMB substrates for the first time. Pure CeO_2 nanoparticles in absence of zeolite Y and their mechanical mixture composites were prepared for comparison. The catalyst of $20CeO_2$/Y nanocomposite demonstrated a robust peroxidase-mimicking activity and stability toward TMB oxidation in presence of

H_2O_2. A sensitive and stable colorimetric assay could be constructed to accurately detect H_2O_2 and glucose in buffer or real blood serum samples, with the detection limits of 0.323 μM and 35.4 μM, respectively. Good chemical stability, high catalytic activity and low costs endow the enzyme mimic of CeO_2/Y nanocomposites with an attractive potential as a commercial glucose detector in real physiological systems.

2. Experimental section

2.1. Chemicals and materials

Cerium(III) nitrate hexahydrate ($Ce(NO_3)_3{\cdot}6H_2O$), hydrogen peroxide (H_2O_2, 30%), TMB (3,3′,5,5′-tetramethylbenzidine), sodium acetate (NaAc), glucose, glucose oxidase (GOx, 2 mg· mL^{-1}) were purchased from Sigma-Aldrich. All reagents above were of analytical grade and used without further purification. The standard zeolite samples of Y (CBV712, Si/Al=10), ZSM-5 (CBV2314, Si/Al=11.5) and mordenite (CBV21A, Si/Al=10) were purchased from Zeolyst International. Sodium acetate buffer (0.2 M, pH=3.6) and phosphate buffer saline (PBS, 0.1 M, pH=7) were freshly prepared.

2.2. Synthesis of CeO_2/Y nanocomposites with different contents of CeO_2

The CeO_2/Y nanocomposites with various contents of CeO_2 (5, 10, 15, 20, 25, 30 wt%, denoted as *x*CeO_2/Y nanocomposites, *x* = mass ratio of CeO_2 to zeolite Y (%)) were prepared by a wet impregnation method [42]. In a typical synthesis of 20CeO_2/Y nanocomposite, 0.76 g of $Ce(NO_3)_3{\cdot}6H_2O$ was dissolved in 15 mL distilled water and mixed with 1.5 g of zeolite Y. Afterwards, the suspension was continuously stirred at room temperature for 5 h, which was then completely dried by infrared lamp under stirring. The obtained product was sequentially dried in an oven overnight at 70°C. Finally, the collected powder was annealed through calcination in a muffle furnace at 600°C for 3 h. Similarly, CeO_2 nanoparticles were obtained by directly calcining $Ce(NO_3)_3{\cdot}\ 6H_2O$ in a muffle furnace at 600°C for 3 h. For comparison, the mechanical mixture sample of CeO_2 nanoparticles and zeolite Y, denoted as 20CeO_2/Y-mix, was obtained through mixing 0.3 g of CeO_2 nanoparticles synthesized

above and 1.5 g of zeolite Y in 5 mL ethanol solution with grinding for 15 min, then the composite was dried at 60^{o}C overnight.

2.3. Characterizations

Powder X-ray diffraction (XRD) patterns were recorded by a Bruker D8 powder X-ray diffractometer (Bruker AXS, German) using Cu K_{α} radiation (40 kV, 40 mA, λ = 1.5406 Å) in the angle range from 5^{o} to 60^{o}/2θ with a scan rate of 0.02°/min. Transmission electron microscopy (TEM) images were taken with a JEM 2011F microscope (JEOL, Japan) operating at 200 kV. Before measurements, the samples were dispersed in ethanol and then dried on a holey carbon film supported Cu grid. The content of CeO_2 in *x*CeO_2/Y nanocomposites was determined by Energy-dispersive X-ray spectroscopy (EDX) as an attachment of TEM. The Brunauer-Emmet-Teller (BET) surface area, total pore volume, and average pore size of samples were measured on a Tristar 3000 instrument (Micromeritics, USA) at liquid nitrogen temperature (77 K). Before measurement, the samples were degassed in vacuum at 180°C for at least 6 h. X-ray photoelectron spectroscopy (XPS) measurements were conducted on a Shimadzu/Kratos AXIS Ultra DLD spectrometer using Al K_{α} radiation (1486.7 eV) as the excitation source. UV-vis absorption spectra were recorded on a YOKE UV-Vis spectrophotometer (UV1900PC, China) with a 0.5 cm UV cell.

2.4. Methods for the peroxidase catalytic activity study

The peroxidase catalytic reaction was performed at 25°C using 0.2 mg CeO_2/Y nanocomposites in 3 mL of sodium acetate buffer (0.2 M, pH=3.6) containing 200 μL TMB (3 mM) as substrate and 100 μL H_2O_2 (100 μM), unless otherwise stated. Similarly, the catalytic activity test of 0.2 mg CeO_2 nanoparticles or CeO_2/Y-mix was performed under the same conditions. The time-dependent absorbance changes at 652 nm were consecutively recorded within 10 min, and the absorbance at 652 nm after 10 min were also immediately measured. The optimum catalyst concentration was screened by using different amounts of 20CeO_2/Y nanocomposite from 0 to 1 mg under the condition of 25°C in 3 mL acetate buffer (0.2 M, pH=3.6) with 200 μL TMB (3 mM) and 100 μL H_2O_2 (100 μM). The pH dependence analysis was

conducted using diverse buffers with pH ranging from 1 to 12, including glycine-HCl buffer (pH 1.0-2.0), acetate buffer (pH 3.0-5.0), phosphate buffer (pH 6.0-8.0), carbonate buffer (pH 9.0-11.0) and glycine-NaOH buffer (pH 12). The temperature dependence analysis was implemented at the temperature ranging from 15°C to 65°C. The stability test was carried out under the generic conditions within one week.

The steady-state kinetic assays with TMB as the substrate were performed using 0.2 mg of 20CeO_2/Y nanocomposite catalyst containing various concentrations of TMB (0.25, 0.5, 0.75, 1, 1.5, 2 and 3 mM) and a constant concentration of 100 μL H_2O_2 (100 μM). Likewise, the kinetic analysis with H_2O_2 as the substrate was also performed using 0.2 mg of 20CeO_2/Y nanocomposite catalyst with different concentrations of H_2O_2 (10, 30, 50, 70, 90 and 130 μM) and a fixed concentration of 200 μL TMB (3 mM). The apparent kinetic parameters were calculated using Lineweaver-Burk plots of the double reciprocal of the Michaelis-Menten equation, $1/V = K_m/V_m(1/[S] + 1/K_m)$, where V is the initial velocity, V_m represents the maximal reaction velocity, [S] corresponds to the concentration of substrate, and K_m is the Michaelis-Menten constant [43-45]. The catalytic constant value (k_{cat}) is used to measure the enzymatic catalytic activity [17].

2.4. Colorimetric detection of H_2O_2 and glucose

The limit of detection (LOD) of H_2O_2 was tested as follows: 0.2 mg of 20CeO_2/Y nanocomposite catalyst, 200 μL of TMB (3 mM), and H_2O_2 with different concentrations (1-300 μM) were added into 3 mL of sodium acetate buffer (0.2 M, pH 3.6). Afterwards, the absorbance of the mixed solutions at 652 nm was measured at room temperature after 10 min.

Similarly, the LOD of glucose was determined as follows. First, 200 μL of glucose solution with various concentrations of 1 μM-5 mM was added into 1 mL of PBS (pH 7.0), and 100 μL of GOx (2 mg· mL^{-1}) was added into each neutral solution. Then, the solutions were incubated at 37°C for 1 h. Subsequently, 0.2 mg of 20CeO_2/Y nanocomposite catalyst, 200 μL of TMB (8 mM), and 2 mL of sodium acetate buffer (0.2 M, pH 3.6) were added into the above solutions. After reaction at 37°C for 1 h, the absorbance of the final solutions at 652 nm were measured at room temperature.

In controlled experiments, 100 μL of 0.5 mM glucose, 5 mM fructose, 5 mM sucrose, and 5 mM lactose were used for a comparison purpose, respectively. The other conditions are the same with that of glucose determination described above. For the determination of glucose in spiked foetal bovine serum, the sample was first centrifuged at 9000 rpm for 1 h, and then the supernatant was diluted in 50 folds for the experiment. The other conditions are the same with that for glucose determination above.

3. Results and discussion

3.1 Structure characterizations

The typical diffraction peaks of zeolite Y (FAU type) appear in its XRD pattern (Figure 1a), which are well remained after loading or mixing with CeO_2 nanoparticles (Figure 1b and 1c). The additional diffraction peaks, centered at 28.7°, 33.1°, 47.6°, 56.4° and 59.1°/2θ are in accord with the characteristic planes (111), (200), (220), (311) and (222) of CeO_2 in the cubic fluorite structure (JCPDS: 81-0792), respectively (Figure 1 and S1). The sample of $20CeO_2$/Y shows more broadening diffraction peaks of CeO_2 in comparison with pure CeO_2 nanoparticles and $20CeO_2$/Y-mix (Figure S1), indicating that $20CeO_2$/Y has the smallest CeO_2 nanoparticles highly decorated on zeolite Y. When CeO_2/Y mass ratio is below 5%, no obvious diffraction peaks of CeO_2 are observed (Figure S2-a), due to low content and high dispersion of CeO_2 nanoparticles on zeolite Y. The peak intensity of zeolite Y decreases, otherwise, the reflection peaks of CeO_2 are enhanced, which become much narrower as the CeO_2/Y mass ratio rises from 10% to 30% (Figure S2), indicating that the particle size of decorated CeO_2 gradually increases.

Nitrogen sorption isotherms of zeolite Y and $20CeO_2$/Y nanocomposite show the typical Type I curves (Figure 2), that are mainly attributed to priority filling of nitrogen molecules in zeolite micropores at low relative pressure. The hysteresis loops prove the presence of mesoporous structures in both samples, stemming from the accumulation of zeolite or CeO_2 nanocrystals. The specific BET surface area and pore volume of parent zeolite Y are estimated to be 747 $m^2 \cdot g^{-1}$ and 0.487 $cm^3 \cdot g^{-1}$,

respectively, providing rich interface for uniform dispersion of CeO_2 nanoparticles. The sample of $20CeO_2$/Y owns lower specific BET surface area (517 $m^2 \cdot g^{-1}$) and pore volume (0.329 $cm^3 \cdot g^{-1}$), indicating the blockage of partial micropores of zeolite Y by deposited CeO_2 nanoparticles.

TEM image of parent zeolite Y (Figure 3a) shows some quadrilateral or pentagonal single crystals about 500 nm in size, presenting the typical morphology of zeolite Y and rough surface observed in FESEM image (Figure S3-a). A great number of CeO_2 nanoparticles with an average size of 5-10 nm are well decorated on the surface of $20CeO_2$/Y (Figure 3b-d), and no separated bulky CeO_2 particles are found. FESEM and HAADF-STEM images also support the same observations (Figure S3-b and c), indicating that CeO_2 species can be spontaneously dispersed without obvious self-agglomeration on zeolite Y after calcination. HRTEM image of $20CeO_2$/Y nanocomposite in Figure 4A reveals the fine crystalline structure of CeO_2 nanocrystals. Some clear lattice fringes with a lattice spacing values of 0.31 nm and 0.19 nm can be seen, which are corresponding to [111] and [220] planes of CeO_2, respectively [45-47]. The SAED pattern (inset in Figure 4A) with distinct diffraction spots, attributed to the lattice fringes [111], [200], and [220] of CeO_2, further confirming the crystalline structures of CeO_2 decorated on zeolite Y. However, pure CeO_2 easily aggregates into the nanoparticles in larger size of 10-20 nm by calcination (Figure S4-b), due to the absence of a proper support for dispersing and stabilizing them in size below 10 nm (Figure S4-a). CeO_2 further grows up and aggregates into particles larger than 30 nm when mixed with zeolite Y by mechanical grinding (Figure 3e and 3f), showing lower dispersity and weaker chemical interaction between CeO_2 and zeolite Y only through mechanical mixing.

In order to evaluate the role of CeO_2 and the valence state of Ce element in $20CeO_2$/Y nanocomposite, high-resolution Ce 3d XPS spectrum for CeO_2 was recorded (Figure 4B). The binding energy values in the range from 880 eV to 920 eV are consistent with those reported before [5], that are from hybridization of O 2p valence band and Ce 4f level. On account of the spin-orbit coupling of $3d_{3/2}$ and $3d_{5/2}$ orbitals, Ce 3d spectrum is well resolved into six fitting peaks. The signs of Ce^{4+} are

marked as four peaks at 918.7 eV (a), 903.1 eV (c), 900.6 eV (d) of Ce $3d_{3/2}$ and 885.1 eV (f) of Ce $3d_{5/2}$, respectively. The peaks centered at 907.7 eV (b) and 889.5 eV (e) can be attributed to Ce^{3+} ions, which come out from Ce $3d_{3/2}$ and Ce $3d_{5/2}$ ionization, respectively. XPS analysis above reveals that both Ce^{3+} and Ce^{4+} ions coexist in $20CeO_2$/Y. According to their corresponding integral areas, the content of Ce^{3+} is calculated to be as high as 35.7%, which is largely helpful for increasing the efficiency of CeO_2 in peroxidase-mimicking catalytic reactions [37].

3.2 Peroxidase-like activity of CeO_2/Y nanocomposites

The intrinsic peroxidase-like activity of $20CeO_2$/Y nanocomposite was examined by the catalytic oxidation of TMB, a typical peroxidase substrate, in the presence and absence of H_2O_2, monitored by the absorption spectroscopy (Figure 5A). An obvious color change from colorless (TMB) into blue solution (ox TMB) can be clearly observed by naked eyes during the reaction; therefore, the peak intensity of ox TMB at 652 nm can be used to evaluate the peroxidase-like catalytic activity over a reaction period of 10 min. In the absence of H_2O_2 and/or the catalyst of $20CeO_2$/Y, negligible absorption at 652 nm was observed (Figure 5A-a to c), indicating that only H_2O_2 or catalyst cannot perform the peroxidase-like reaction toward TMB. In contrast, the system of TMB+$20CeO_2$/Y+H_2O_2 presents a strong absorption at 652 nm under the same conditions (Figure 5A-d), revealing a great catalytic activity of $20CeO_2$/Y in the presence of H_2O_2. Pure CeO_2 nanoparticles and $20CeO_2$/Y-mix show lower catalytic activity for comparison (Figure 5B). In fact, the amount of CeO_2 in pure CeO_2 nanoparticles is 5 times of that in $20CeO_2$/Y. When the quality of pure CeO_2 nanoparticles decreases from 0.2 mg to 0.04 mg in the reaction, the relative activity decreases from 35.6% to only 8.3%. Therefore, CeO_2 nanoparticles of 5-10 nm in size highly decorated on zeolite Y perform superior catalytic activity in TMB oxidation. To further search for the influence of supporting matrix, zeolites of mordenite (MOR type) and ZSM-5 (MFI type) with the same Si/Al ratios as zeolite Y but slightly hydrophobic surface were used to load CeO_2. Lower relative activity of $20CeO_2$/MOR and $20CeO_2$/ZSM-5 further indicates that CeO_2 particles in size larger than 30 nm almost have no peroxidase-like catalytic activity even dispersed on zeolite support

(Figure S5 and S6). Therefore, only highly dispersed CeO_2 nanoparticles in size below 10 nm can perform as the active catalyst in H_2O_2 decomposition and TMB oxidation. In order to achieve this purpose, zeolite Y is chosen as the optimal support, on which CeO_2 nanoparticles of 5-10 nm can be stably loaded with uniform dispersion.

Because the number of active sites provided by CeO_2 nanoparticles affect the catalytic efficiency, the peroxidase-like activity of CeO_2/Y nanocomposites with various CeO_2 contents as well as different catalyst amount was investigated in detail (Figure 6). With CeO_2/Y mass ratio increasing from 5% to 20%, the relative activity is gradually enhanced from 50% to 100% (Figure 6a), due to the increasing of active sites exposed on zeolite surface before the CeO_2 loading threshold of 20%. As further increase of CeO_2 loading from 20% to 30%, the CeO_2/Y nanocomposites show a decreasing peroxidase-like activity, even lower than 40%. The reduction of catalytic activity is mainly caused by the aggregation and low dispersion of excessive CeO_2 particles on zeolite Y. This further proves that CeO_2 nanoparticles smaller than 10 nm are beneficial to the peroxidase-like reaction. Therefore, the sample of CeO_2/Y nanocomposite with mass ratio of 20% is the optimal catalyst as the peroxidase-mimicking nanozyme toward TMB oxidation. Moreover, the catalytic activity is also dependent on the quality of 20CeO_2/Y nanocomposite added in the reaction (Figure 6b). The absorbance at 652 nm increases sharply within 0.2 mg, but nearly remains unchanged from 0.2 mg to 1.0 mg of catalysts. Thus 0.2 mg of 20CeO_2/Y catalyst is the most suitable quality, presenting enough active sites for the peroxidase-like catalytic reaction toward TMB.

In addition, the catalytic activity of 20CeO_2/Y nanocomposite depends on the reaction conditions such as pH and temperature, similar to that of other peroxidase-like mimics or the natural enzyme HRP [38]. The peroxidase-like activity of 20CeO_2/Y nanocomposite was investigated by varying pH values from 1.0 to 12 and temperatures from 15^{o}C to 65^{o}C (Figure 7). When pH value increases from 1.1 to 3.6 (Figure 7a), the relative activity rapidly increases from 12.5% to 100%, but it sharply decreases with pH varying from 3.6 to 12. Therefore, the optimal pH is about

3.6. Because strong acidic (pH<3.6) or alkaline (pH>7) conditions are not beneficial for CeO_2 acting as catalyst for the decomposition of surface peroxide species. The produced hydroxyl radicals are very reactive to oxidize TMB into blue oxidized TMB quickly. It's well known that reaction temperature is one of the most important factors affecting the performance of peroxidase catalysts. The enzyme HRP can work with high efficiency only in a very narrow temperature range from 20°C to 30°C. From Figure 7b, it can be seen that the reaction rate of $20CeO_2$/Y nanocomposite increases gradually with temperatures, indicating that the catalyst possesses a good temperature resistance. The quite commendable catalytic activity can be remained even at the temperature higher than 50°C with self-decomposition of partial H_2O_2. Furthermore, the stability test of $20CeO_2$/Y nanocomposite was carried out for one week (Figure S7). The relative activity has no obvious loss in each test, and it can approach higher than 90% after recycle use for 7 times, showing a great stability and repeatability as the peroxidase-like catalyst.

3.3 Kinetic studies of the peroxidase-like activity of CeO_2/Y nanocomposites

In order to explore the mechanism of the peroxidase-like activity, the typical Michaelis-Menten curves are obtained for the catalyst of $20CeO_2$/Y nanocomposite within the suitable concentration range of TMB (Figure 8a) and H_2O_2 (Figure 8c) as substrates, respectively. The apparent steady-state kinetic parameters (K_m and V_{max}) were obtained by the initial reaction rate method under the optimal conditions (pH=3.6 and temperature of 25°C), which were highly consistent with the values evaluated from the Lineweaver-Burk double-reciprocal plots (Figure 8b and 8d) [44]. As shown in Table 1, the K_m value of $20CeO_2$/Y catalyst with TMB as substrate was 1.52 mM, lower than that of horseradish peroxidase (HRP) reported before [48], suggesting that $20CeO_2$/Y nanocomposite as the peroxidase-mimicking catalyst has a better affinity for TMB than HRP, probably due to the large surface area and pore volume of porous zeolite Y with a strong adsorption ability to TMB as well as the uniform dispersion of CeO_2 nanoparticles in size of 5-10 nm. Moreover, the K_m value of $20CeO_2$/Y with H_2O_2 as substrate was 0.15 mM, one fourth of the K_m value of HRP, indicating that a lower H_2O_2 concentration was required for $20CeO_2$/Y than that for

HRP to achieve the maximum activity. Therefore, from the apparent steady-state kinetic analysis, we can see that the $20CeO_2$/Y nanocomposite has higher activity and sensitivity than HRP, toward TMB oxidation as the peroxidase-like catalyst. The derived catalytic constant (k_{cat}) was also taken to compare the enzymatic catalytic activity. The k_{cat} values of $20CeO_2$/Y with TMB and H_2O_2 as the substrates are 0.164 min^{-1} and 51.6 min^{-1}, respectively, higher than that of HRP (0.019 min^{-1} and 2.14 min^{-1}), showing an excellent catalytic efficiency of $20CeO_2$/Y nanocomposite as a peroxidase mimic.

3.4 Detection of H_2O_2 and glucose detection using $20CeO_2$/Y nanocomposite

It's well known that H_2O_2 and glucose detections are well applied in the biomedicine diagnosis and food research [49]. Owing to the promising peroxidase-like activity of $20CeO_2$/Y nanocomposite, a simple colorimetric method was set up to detect the concentration of H_2O_2 and glucose in solution. The absorbance of oxidized TMB is dependent on the H_2O_2 concentration from 1 to 300 μM under the optimal conditions (Figure S8 and 9a). Figure 9b presents a good linear relationship between the absorbance of oxidized TMB and H_2O_2 concentration in the range of 0-5 μM with a detection limit of 0.323 μM. In comparison with the other CeO_2-based peroxidase mimics reported before, the catalyst of $20CeO_2$/Y nanocomposite shows a relatively narrow linear range but a very low detection limit of H_2O_2 [38]. In glucose detection, glucose is firstly oxidized into gluconic acid and hydrogen peroxide under the catalytic action of glucose oxidase (GOx). Afterwards, TMB can be oxidized by the generated hydrogen peroxide through catalysis action of $20CeO_2$/Y nanocomposite. Subsequently, the blue product deriving from the oxidized TMB can be employed to detect the content of glucose. The results of glucose detection are shown in Figure 10 and S9, in which the absorbance of oxidized TMB is gradually increased with glucose concentration and an obvious color change is observed. As illustrated in Figure 10b, the absorbance is linearly correlated to glucose concentration from 0 to 340 μM with a detection limit of 35.4 μM. Compared to the reported CeO_2-based glucose biosensors by the colorimetric method, $20CeO_2$/Y nanocomposite presents a slightly higher detection limit but a wide linear range of

glucose [7]. In addition, the selectivity to different sugars was investigated in Figure 11. Owing to the specificity of GOx towards glucose, the colorimetric method has a very weak response to the other tested sugars, such as fructose, sucrose and lactose in the solution, showing the superior selectivity to glucose detection using $20CeO_2/Y$ nanocomposite as the peroxidase-like catalyst. Furthermore, the glucose content in the real sample of foetal bovine serum (FBS) was detected by this method (Figure 12). According to the calibration curve in Figure 10b, the concentration of glucose in the spiked FBS sample is calculated to be about 4.8 mM, in good agreement with that determined by a spectrophotometric method (5.0 mM), indicating that the colorimetric method using $20CeO_2/Y$ nanocomposite as the peroxidase mimics possesses a high reliability for glucose detection in human serums. The superior peroxidase-mimicking performance of CeO_2/Y nanocomposite can be attributed to the synergistic effects of outstanding activity of highly dispersed CeO_2 nanoparticles and high surface area and pore volume of zeolite Y as support. Firstly, zeolite Y is an ideal support, which supplies proper interface for uniform dispersion of CeO_2 nanoparticles. Secondly, CeO_2 nanoparticles in size of 5-10 nm show high reactivity and long stability in H_2O_2 decomposition and TMB oxidation, due to their special composition of Ce^{3+} and Ce^{4+} and the confinement effect of zeolite Y support. Thirdly, zeolite Y owns very large surface area and pore volume, which can enhance the adsorption ability of TMB and H_2O_2 on the surface of catalyst.

Conclusions

In summary, CeO_2 nanoparticles-decorated zeolite Y nanocomposites were prepared by a conventional wet impregnation method. The hybrid CeO_2/Y nanomaterials were performed as a peroxidase-mimicking nanozyme for the detection of H_2O_2 and glucose, due to their synergistic effects of outstanding activity of highly dispersed CeO_2 nanoparticles (5-10 nm in size) and large surface area (517 $m^2 \cdot g^{-1}$) and pore volume (0.329 $cm^3 \cdot g^{-1}$) of zeolite Y as support. Moreover, the optimized combination of zeolite Y and CeO_2 presents high contents of Ce^{3+} species (35.7%),

which are beneficial to generate a large number of hydroxyl radicals as well as enhance the catalytic performance as a peroxidase-like mimic. The activity of the CeO_2/Y peroxidase-mimicking catalyst is dependent on the support types (zeolite Y, ZSM-5, mordenite), CeO_2 sizes and contents, catalyst amount, pH, temperature, H_2O_2 and TMB concentration. In addition, the catalyst of 20CeO_2/Y nanocomposite, with CeO_2/zeolite Y mass ratio equal to 0.20 and CeO_2 particle size of 5-10 nm, shows higher affinity to TMB and H_2O_2 than HRP, and exhibits the excellent peroxidase-mimicking activity under the conditions of pH=3.6 and a broad temperature range from 15℃ to 65℃. Therefore, a facile colorimetric assay could be set up for the detection of H_2O_2 with a narrow linear range (0-5 μM) but a very low detection limit (0.323 μM). The method could also be used as a glucose biosensor, with a slightly higher detection limit (35.4 μM) but a wide linear range (0 to 340 μM). The 20CeO_2/Y nanocomposite shows a high selectivity to glucose against other sugars, which could be utilized to accurately detect the glucose concentration in real blood serum samples. The colorimetric assay based on the low-cost and high-efficiency CeO_2/Y nanocomposites has a potential application in biochemical analysis, clinical diagnosis, environmental monitoring, food detection, and so on.

Acknowledgments

This work was sponsored by Shanghai Pujiang Program, China (No. 16PJ1401100), and the Shanghai Committee of Science and Technology, China (No. 15ZR1402000), Key Basic Research Program of Science and Technology Commission of Shanghai Municipality (17JC1400100), the NSF of China (21673048), National Youth Top Talent Support Program of National High-Level Personnel of Special Support Program (Youth Top-notch Talent Support Program).

References

[1] R. Wolfenden, M. J. Snider, The depth of chemical time and the power of

enzymes as catalysts. Acc. Chem. Res. 34 (2001) 938-945.

[2] Y. Chen, H. Cao, W. Shi, H. Liu, Y. Huang, Fe-Co bimetallic alloy nano-particles as a highly active peroxidase mimetic and its application in biosensing. Chem. Commun. 49 (2013) 5013-5015.

[3] A. K. Dutta, S. K. Maji, D. N. Srivastava, A. Mondal, P. Biswas, P. Paul, B. Adhikary, Synthesis of FeS and FeSe nanoparticles from a single source precursor: a study of their photocatalytic activity, peroxidase-like behavior, and electrochemical sensing of H_2O_2. ACS Appl. Mater. Interfaces 4 (2012) 1919-1927.

[4] F. Qiao, L. Chen, X. Li, L. Li, S. Ai, Peroxidase-like activity of manganese selenide nanoparticles and its analytical application for visual detection of hydrogen peroxide and glucose. Sens. Actuators B. 193 (2014) 255-262.

[5] W. Y. Yin, J. Yu, F. T. Lv, L. Yan, L. R. Zheng, Z. J. Gu, Y. L. Zhao, Functionalized nano-MoS_2 with peroxidase catalytic and near-infrared photothermal activities for safe and synergetic wound antibacterial applications. ACS Nano. 10 (2016) 11000-11011.

[6] L. Jin, Z. Meng, L. Shang, Ultra small Pt nanoclusters as robust peroxidase mimics for colorimetric detection of glucose in human serum. ACS Appl. Mater. Interfaces 9 (2017) 10027-10033.

[7] D. Jampaiah, T. S. Reddy, S. K. Bhargava, Fe-doped CeO_2 nanorods for enhanced peroxidase-like activity and their application towards glucose detection. J. Mater. Chem. B. 4 (2016) 3874-3885.

[8] A. Dalui, B. Pradhan, U. Thupakula, A. H. Khan, G. S. Kumar, T. Ghosh, B. Satpati, S. Acharya, Insight into the mechanism revealing the peroxidase mimetic catalytic activity of quaternary CuZnFeS nanocrystals: colorimetric biosensing of hydrogen peroxide and glucose. Nanoscale. 7 (2015) 9062-9074.

[9] H. Cheng, S. Lin, F. Muhammad, Y. W. Lin, H. Wei, Rationally modulate the oxidase-like activity of nanoceria for self-regulated bioassays. ACS Sensors. 1 (2016) 1336-1343.

[10] Y. H. Li, J. S. Ren, X. G, Qu, Catalytically active nanomaterials: a promising candidate for artificial enzymes. Acc. Chem. Res. 47 (2014) 1097-1105.

[11] X. Y. Wang, Y. H. Hu, H. Wei, Nanozymes in bionanotechnology: from sensing to therapeutics and beyond. Inorg. Chem. Front 3 (2016) 41-60.

[12] G. Wang, X. Xu, L. Qiu, Y. Dong, Z. Li, C. Zhang, Dual responsive enzyme mimicking activity of AgX (X = Cl, Br, I) nanoparticles and its application for cancer cell detection. ACS Appl. Mater. Interfaces 6 (2014) 6434-6442.

[13] X. Hu, A. Saran, S. Hou, T. Wen, Y. Ji, W. Liu, H. Zhang, W. He, J. J. Yin, X. Wu, Au@PtAg core/shell nanorods: tailoring enzyme-like activities via alloying. RSC Adv. 3 (2013) 6095-6105.

[14] K. Cai, Z. Lv, K. Chen, L. Huang, J. Wang, F. Shao, Y. Wang, H. Han, Aqueous synthesis of porous platinum nanotubes at room temperature and their intrinsic peroxidase-like activity. Chem. Commun. 49 (2013) 6024-6026.

[15] C. W. Lien, C. C. Huang, H. T. Chang, Peroxidase-mimic bismuth-gold nano-particles for determining the activity of thrombin and drug screening. Chem. Commun. 48 (2012) 7952-7954.

[16] X. X. Wang, Q. Wu, Z. Shan, Q. M. Huang, BSA-stabilized Au clusters as peroxidase mimetics for use in xanthine detection. Biosens. Bioelectron. 26 (2011) 3614-3619.

[17] Y. Tao, Y. H. Lin, Z. Z. Huang, J. S. Ren, X. G. Qu, Incorporating graphene oxide and gold nanoclusters: a synergistic catalyst with surprisingly high peroxidase-like activity over a broad pH range and its application for cancer cell detection. Adv. Mater. 25 (2013) 2594-2599.

[18] H. Chen, Y. Li, F. Zhang, G. Zhang, X. Fan, Graphene supported Au-Pd bimetallic nanoparticles with core-shell structures and superior peroxidase-like activities. J. Mater. Chem. 21 (2011) 17658-17661.

[19] F. Yu, Y. Huang, A. J. Cole, V. C. Yang, The artificial peroxidase activity of magnetic iron oxide nanoparticles and its application to glucose detection. Biomaterials. 30 (2009) 4716-4722.

[20] L. Hu, Y. Yuan, L. Zhang, J. Zhao, S. Majeed, G. Xu, Copper nanoclusters as peroxidase mimetics and their applications to H_2O_2 and glucose detection. Anal. Chim. Acta. 762 (2013) 83-86.

[21] R. Andre, F. Natalio, M. Humanes, J. Leppin, K. Heinze, R. Wever, H. C. Schroder, W. E. G. Muller, W. Tremel, V_2O_5 nanowires with an intrinsic peroxidase-like activity. Adv. Funct. Mater. 21 (2011) 501-509.

[22] Y. Lin, L. Wu, Y. Huang, J. Ren, X. Qu, Positional assembly of hemin and gold nanoparticles in graphene-mesoporous silica nanohybrids for tandem catalysis. Chem. Sci. 6 (2015) 1272-1276.

[23] M. Shamsipur, A. Safavi, Z. Mohammadpour, Indirect colorimetric detection of glutathione based on its radical restoration ability using carbon nanodots as nanozymes. Sens. Actuators B. 199 (2014) 463-469.

[24] L. Su, J. Feng, X. Zhou, C. Ren, H. Li, X.Chen, Colorimetric detection of urine glucose based $ZnFe_2O_4$ magnetic nanoparticles. Anal. Chem. 84 (2012) 5753-5758.

[25] (a) H. Tan, C. Ma, L. Gao, Q. Li, Y. Song, F. Xu, T. Wang, L. Wang, Metal-organic framework-derived copper nanoparticle@carbon nanocomposites as peroxidase mimics for colorimetric sensing of ascorbic acid. Chem. Eur. J. 20 (2014) 16377-16383; (b) R. Ragg, M. N. Tahir, W. Tremel, Solids go bio: inorganic nanoparticles as enzyme mimics. Eur. J. Inorg. Chem. (2016) 1906-1915.

[26] X. Sun, S. Guo, Y. Liu, S. Sun, Dumbbell-like PtPd-Fe_3O_4 nanoparticles for enhanced electrochemical detection of H_2O_2. Nano Lett. 12 (2012) 4859-4863.

[27] S. Mansingh, D. K. Padhi, K. M. Parida, Enhanced visible light harnessing and oxygen vacancy promoted N, S Co-doped CeO_2 nanoparticle: a challenging photocatalyst for Cr (VI) reduction. Catal. Sci. Technol. 7 (2017) 2772-2781

[28] C. Mandoli, F. Pagliari, S. Pagliari, G. Forte, P. D. Nardo, S. Licoccia, E. Traversa, Stem cell aligned growth induced by CeO_2 nanoparticles in PLGA scaffolds with improved bioactivity for regenerative medicine. Adv. Funct. Mater. 20 (2010) 1617-1624.

[29] M. Soh, D. W. Kang, S. H. Lee, T. Hyeon, Ceria-zirconia nanoparticles as an enhanced multi-antioxidant for sepsis treatment. Angew. Chem. Int. Ed. 56 (2017) 11399-11403.

[30] Y. Y. Li, X. He, J. J. Yin, Y. H. Ma, P. Zhang, J. Y. Li, Y. J. Ding, J. Zhang, Y. L. Zhao, Z. F. Chai, Z. Y. Zhang, Acquired superoxide-scavenging ability of ceria

nanoparticles, Angew. Chem. 127 (2015) 1852-1855.

[31] C. Xu, X. Qu, Cerium oxide nanoparticle: a remarkably versatile rare earth nanomaterial for biological applications. NPG Asia Mater. 6 (2014) e90.

[32] C. Walkey, S. Das, S. Seal, J. Erlichman, K. Heckman, L. Ghibelli, E. Traversa, J. F. McGinnis, W. T. Self, Catalytic properties and biomedical applications of cerium oxide nanoparticles. Environ. Sci.: Nano 2 (2015) 33-53.

[33] T. Pirmohamed, J. M. Dowding, S. Singh, B. Wasserman, E. Heckert, A. S. Karakoti, J. E. S. King, S. Seal, W. T. Self, Nanoceria exhibit redox state-dependent catalase mimetic activity. Chem. Commun. 46 (2010) 2736-2738.

[34] E. G. Heckert, A. S. Karakoti, S. Seal, W. T. Self, The role of cerium redox state in the SOD mimetic activity of nanoceria. Biomaterials. 29 (2008) 2705-2709.

[35] A. Asati, S. Santra, C. Kaittanis, S. Nath, J. M. Perez, Oxidase-like activity of polymer-coated cerium oxide nanoparticles. Angew. Chem. Int. Ed. 48 (2009) 2308-2312.

[36] J. Mu, Y. Wang, M. Zhao, L. Zhang, Intrinsic peroxidase-like activity and catalase-like activity of Co_3O_4 nanoparticles. Chem. Commun. 48 (2012) 2540-2542.

[37] H. Zhao, Y. M. Dong, P. P. Jiang, G. L. Wang, J. J. Zhang, Highly dispersed CeO_2 on TiO_2 nanotube: a synergistic nanocomposite with superior peroxidase-like activity. ACS Appl. Mater. Interfaces 7 (2015) 6451-6461.

[38] L. F. Sun, Y. Y. Ding, Y. L. Jiang, Q. Y. Liu, Montmorillonite-loaded ceria nanocomposites with superior peroxidase-like activity for rapid colorimetric detection of H_2O_2. Sens. Actuators B. 239 (2017) 848-856.

[39] M. Choi, K. Na, J. Kim, Y. Sakamoto, O. Terasaki, R. Ryoo, Stable single-unit-cell nanosheets of zeolite MFI as active and long-lived catalysts. Nature. 461 (2009) 246-249.

[40] S. Kulprathipanja, Zeolites in industrial separation and catalysis, Wiley-VCH Verlag GmbH & Co, KGaA Weinheim, 2010.

[41] H. Ramezani, S. N. Azizi, S. R. Hosseini, NaY zeolite as a platform for preparation of Ag nanoparticles arrays in order to construction of H_2O_2 sensor. Sens. Actuators B. 248 (2017) 571-579.

[42] R. B. Zhang, K. Lu, L. J. Zong, S. Tong, X. W. Wang, G. Feng, Gold supported on ceria nanotubes for CO oxidation. Applied Surface Science. 416 (2017) 183-190.

[43] X. Sun, S. Guo, C. S. Chung, W. Zhu, S. Sun, A sensitive H_2O_2 assay based on dumbbell-like PtPd-Fe_3O_4 nanoparticles. Adv. Mater. 25 (2013) 132-136.

[44] Y. L. Dong, H. G. Zhang, Z. U. Rahman, L. Su, X. j. Chen, J. Hu, X. G. Chen, Graphene oxide-Fe_3O_4 magnetic nanocomposites with peroxidase-like activity for colorimetric detection of glucose. Nanoscale. 4 (2012) 3969-3976.

[45] D. Jampaiah, K. M. Tur, S. J. Ippolito, Y. M. Sabri, J. Tardio, S. K. Bhargava, B. M. Reddy, Structural characterization and catalytic evaluation of transition and rare earth metal doped ceria-based solid solutions for elemental mercury oxidation. RSC Adv. 3 (2013) 12963-12974.

[46] D. Jampaiah, S. J. Ippolito, Y. M. Sabri, B. M. Reddy, S. K. Bhargava, Highly efficient nanosized Mn and Fe codoped ceria-based solid solutions for elemental mercury removal at low flue gas temperatures. Catal. Sci. Technol. 5 (2015) 2913-2924.

[47] W. C. Wang,; S. Y. Chen, P. A. Glans, J. Guo, R. J. Chen, K. W. Fong, C. L. Chen, A. Gloter, C. L. Chang, T. S. Chan, J. M. Chen, J. F. Lee, C. L. Dong, Towards understanding the electronic structure of Fe-doped CeO_2 nanoparticles with X-ray spectroscop. Phys. Chem. Chem. Phys. 15 (2013) 14701-14707.

[48] C. Lu, X. J. Liu, Y. F. Li, F. Yu, L. H. Tang, Y. J. Hu, Y. B. Ying, Multifunctional Janus hematite-silica nanoparticles: mimicking peroxidase-like activity and sensitive colorimetric detection of glucose. ACS Appl. Mater. Interfaces 7 (2015) 15395-15402.

[49] S. D. Liu, K. S. Hui, K. N. Hui, Flower-like copper cobaltite nanosheets on graphite paper as high performance super capacitor electrodes and enzymeless glucose sensors. ACS Appl. Mater. Interfaces 8 (2016) 3258-3267.

Figures and Tables

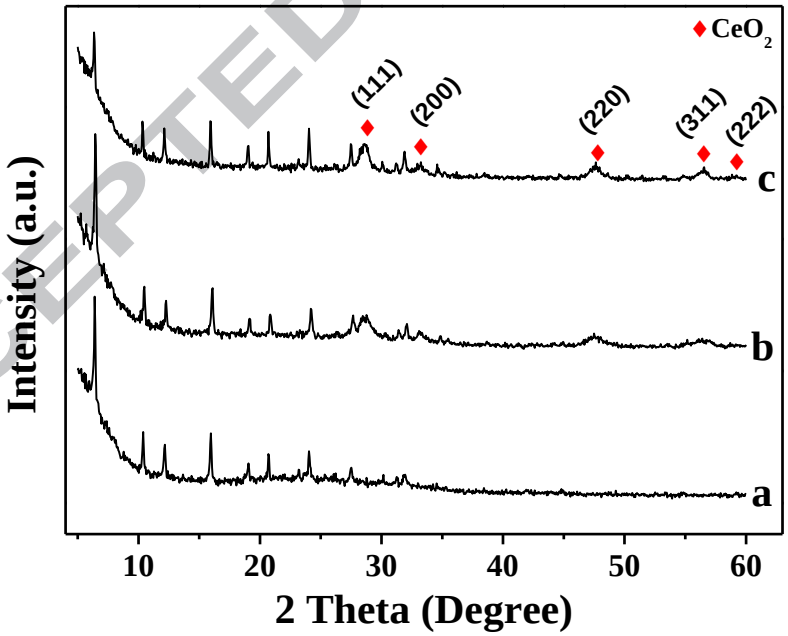

Figure 1. XRD patterns of different samples: (a) parent zeolite Y, (b) 20CeO_2/Y nanocomposite, and (c) 20CeO_2/Y-mix nanocomposite.

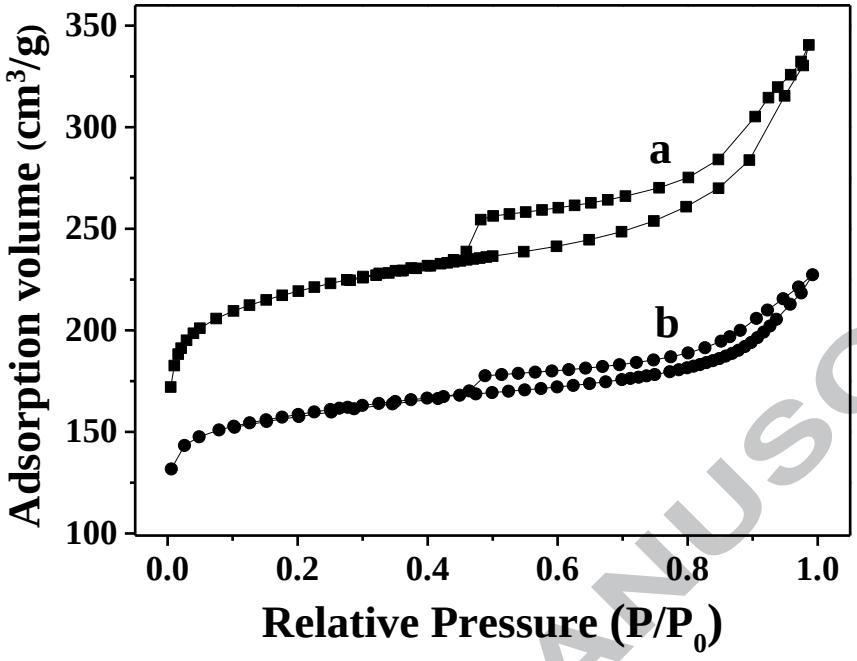

Figure 2. Nitrogen adsorption-desorption isotherm curves of the samples: (a) parent zeolite Y, and (b) 20CeO_2/Y nanocomposite.

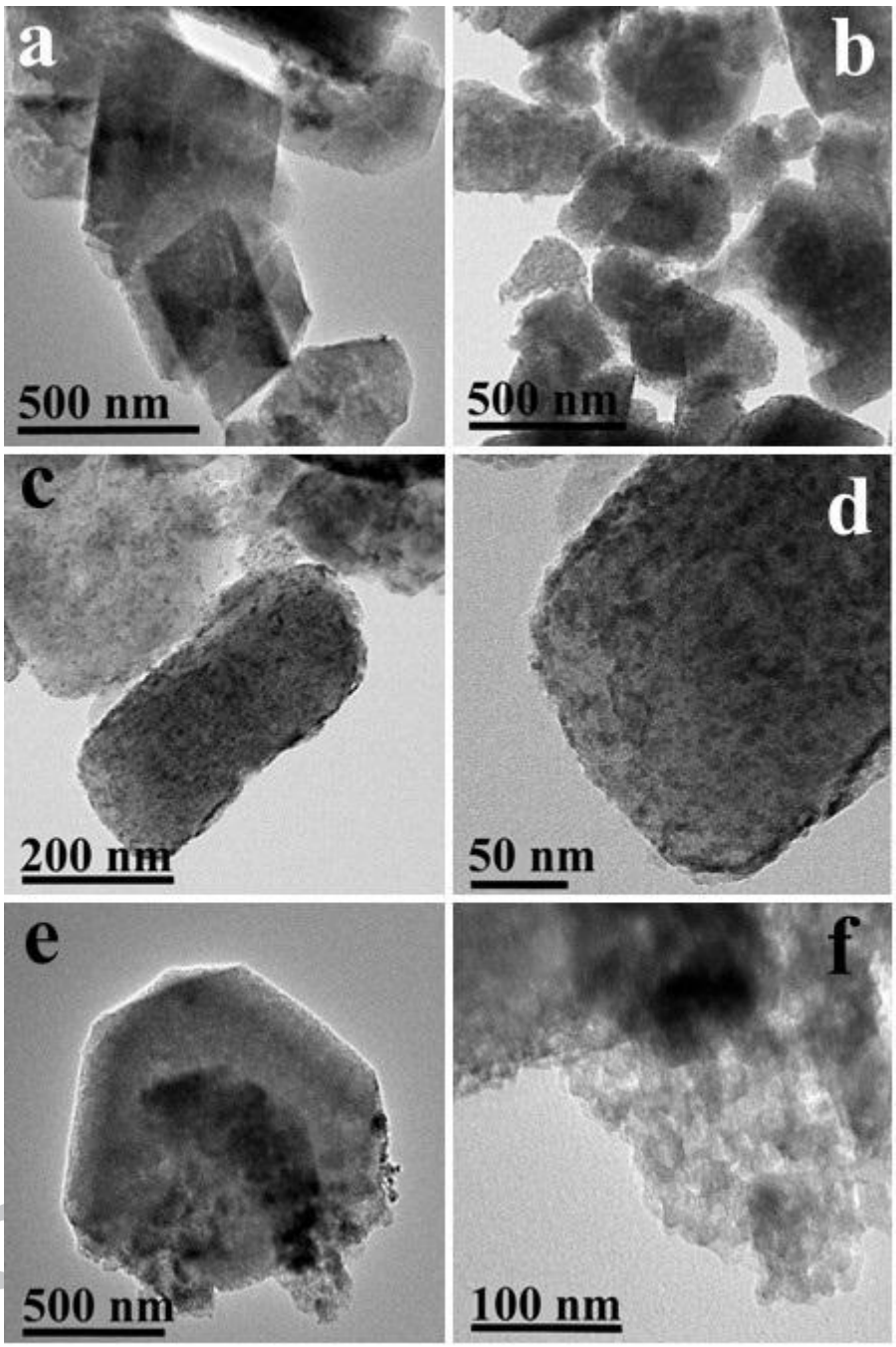

Figure 3. TEM images of the samples: (a) parent zeolite Y, (b, c, d) 20CeO_2/Y nanocomposite, and (e, f) 20CeO_2/Y-mix nanocomposite.

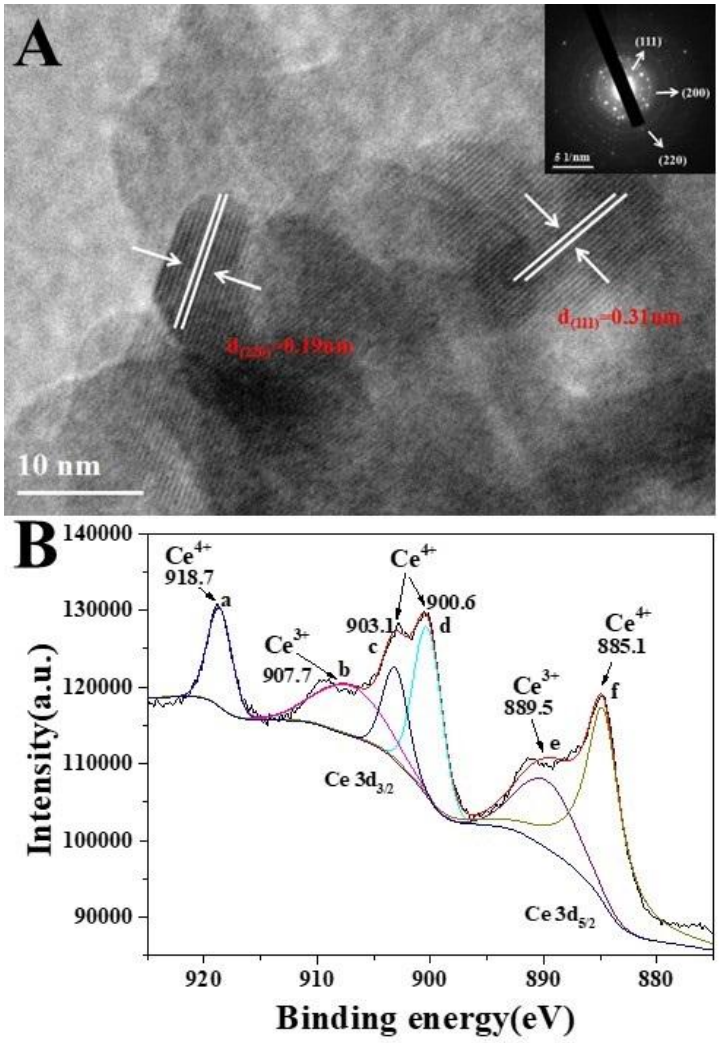

Figure 4. HRTEM image (a) and Ce 3d XPS spectrum (b) of the sample of $20CeO_2$/Y nanocomposite.

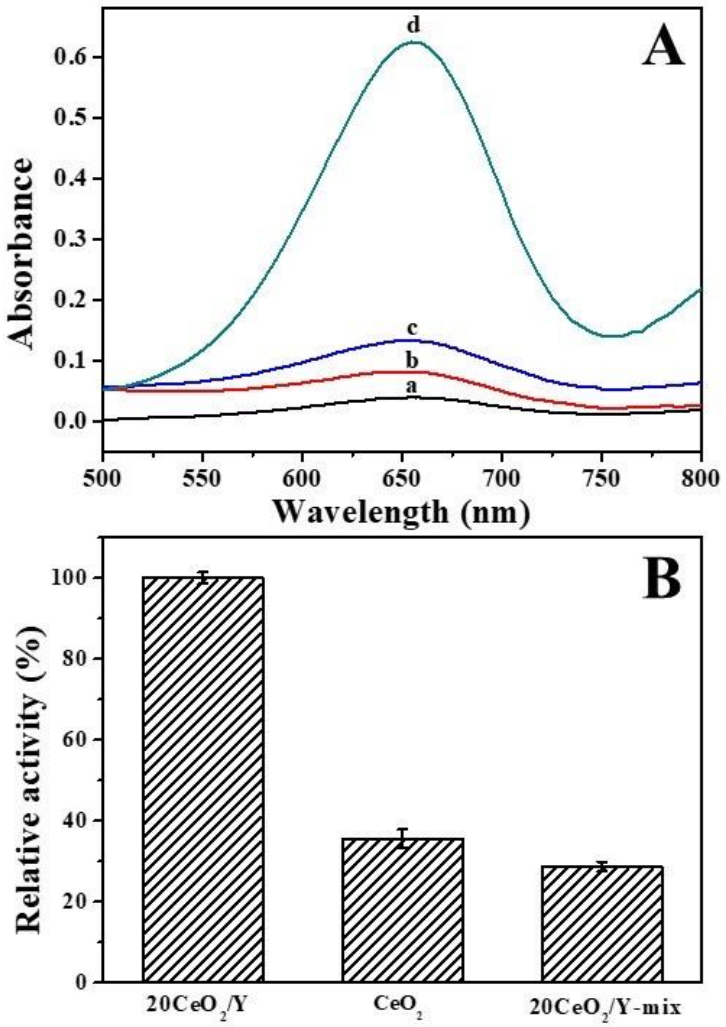

Figure 5. (A) Typical absorption spectra of TMB-H_2O_2 mixed solution in the absence and presence of 20CeO_2/Y nanocomposite catalyst: (a) TMB, (b) TMB+H_2O_2, (c) TMB+20CeO_2/Y, and (d) TMB+20CeO_2/Y+H_2O_2. (B) Relative activity of different types of catalyst samples of 20CeO_2/Y, CeO_2 nanoparticles and 20CeO_2/Y-mix, respectively. Experimental conditions: catalysts: 0.2 mg; acetate buffer: 0.2 M (pH=3.6); TMB: 3 mM; H_2O_2: 100 μM; the reaction mixtures were incubated at 25^{o}C for 10 min, and the absorbance was measured at room temperature.

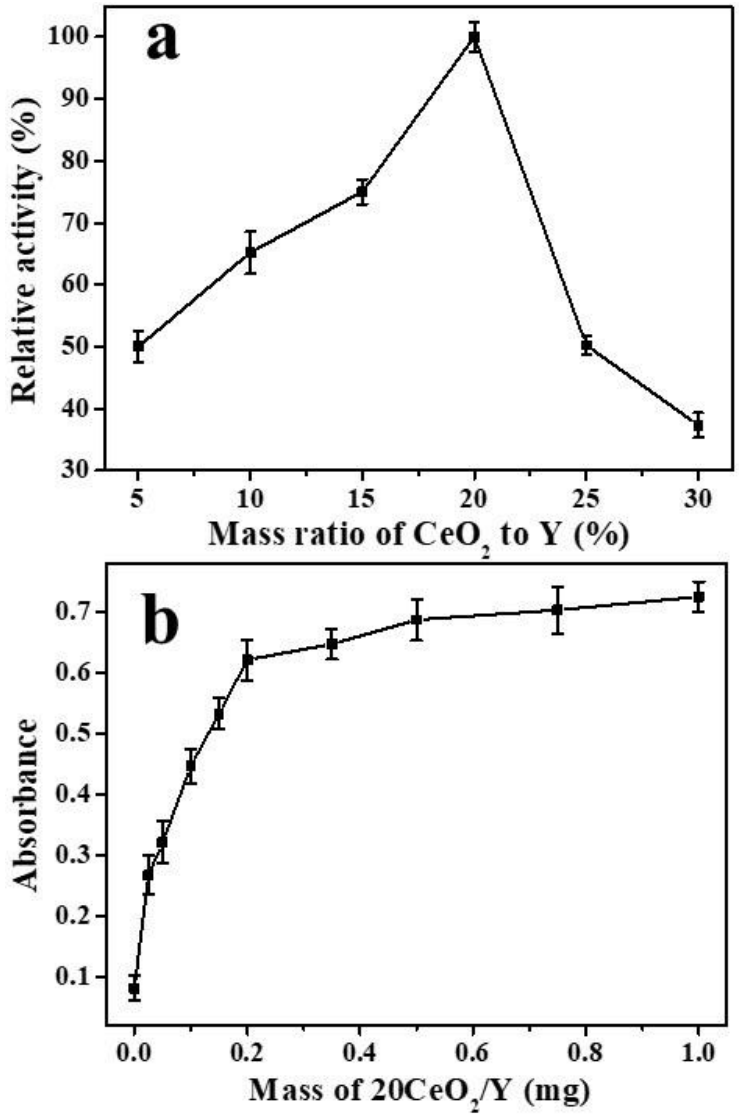

Figure 6. (a) Variations of relative activity of xCeO$_2$/Y nanocomposite catalyst with x from 5% to 30% (catalysts: 0.2 mg), and (b) mass effects of 20CeO$_2$/Y nanocomposite catalyst from 0 to 1.0 mg in the system. Experimental conditions: acetate buffer: 0.2 M (pH=3.6); TMB: 3 mM; H_2O_2: 100 μM; the reaction mixtures were incubated at 25^{o}C for 10 min, and the absorbance was measured at room temperature.

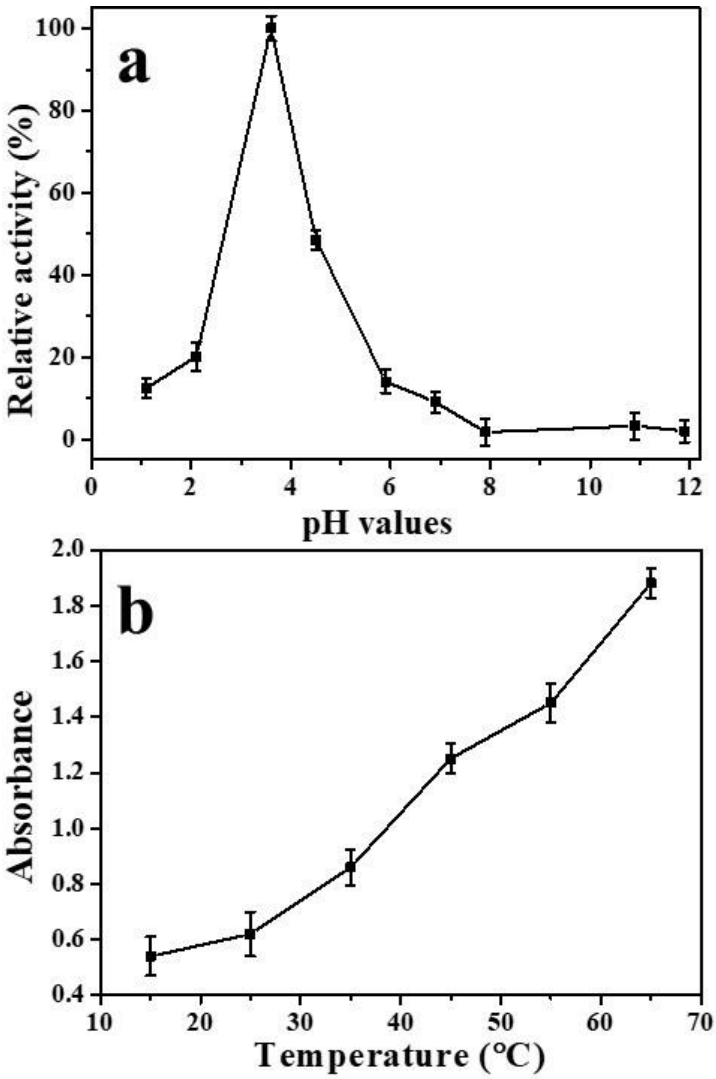

Figure 7. The optimization of pH (a) and temperature (b) for the activity of $20CeO_2$/Y nanocomposite catalyst. Experimental conditions: catalysts: 0.2 mg; TMB: 3 mM; H_2O_2: 100 μM, the absorbance was measured at room temperature.

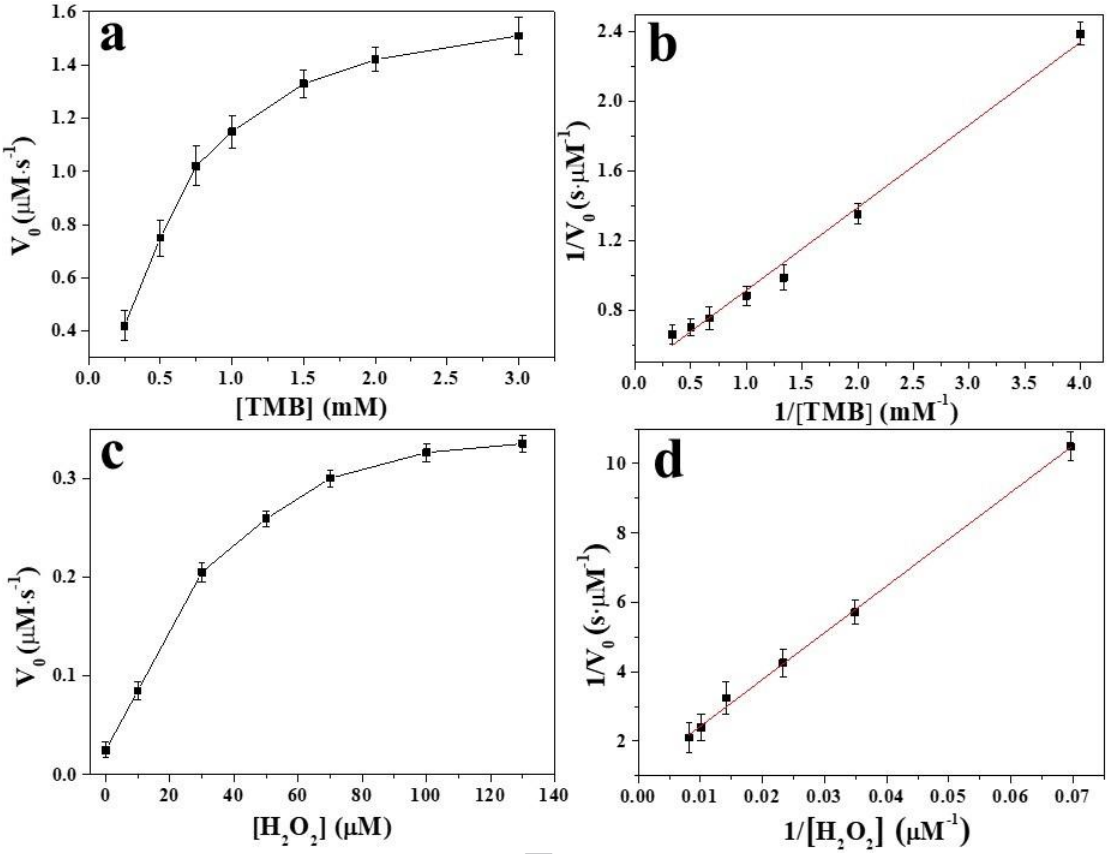

Figure 8. The steady-state kinetic analysis using Michaelis-Menten model (a, c) and Lineweaver-Burk double-reciprocal model (b, d) for $20CeO_2$/Y nanocomposite catalyst. The concentration of H_2O_2 was 100 μM while TMB concentration was altered (a, b). In turn, the concentration of TMB was 3 mM and H_2O_2 concentration was varied (c, d). Other experimental conditions: catalysts: 0.2 mg; acetate buffer: 0.2 M (pH=3.6); the reaction mixtures were incubated at 25^{o}C for 10 min, and the absorbance was measured at room temperature.

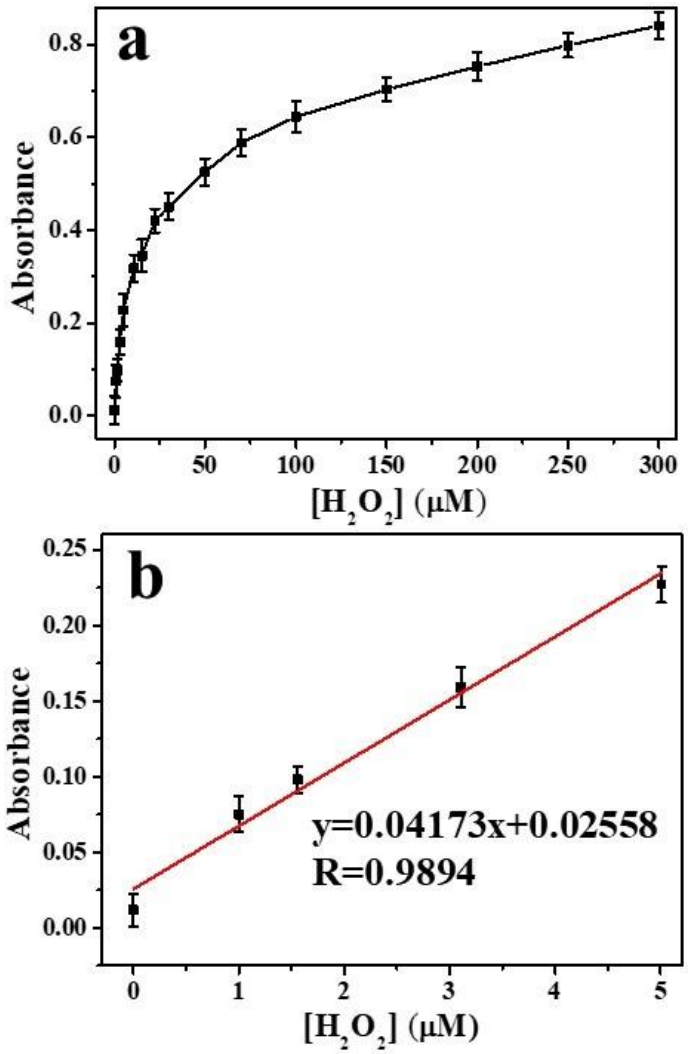

Figure 9. (a) H_2O_2 concentration response curve for H_2O_2 detection using $20CeO_2$/Y nanocomposite catalyst, and (b) the corresponding linear calibration plot for H_2O_2 in the range of 0 to 5 μM. Experimental conditions: catalysts: 0.2 mg; TMB: 3 mM; the reaction mixtures were incubated at 25°C for 10 min, and the absorbance was measured at room temperature.

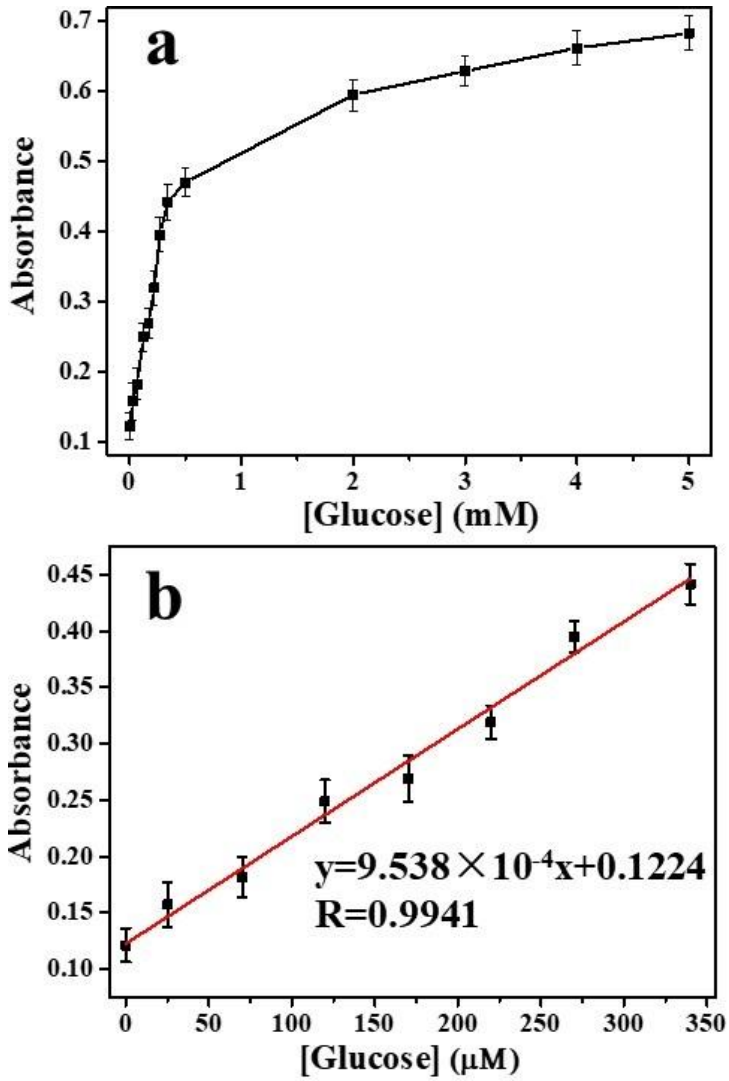

Figure 10. (a) Glucose concentration response curve for glucose detection using $20CeO_2$/Y nanocomposite catalyst, and (b) the corresponding linear calibration plot for glucose in the range of 1 μM to 350 μM. Experimental conditions: catalysts: 0.2 mg; acetate buffer: 0.2 M (pH=3.6); PBS buffer (pH 7.0); TMB, 8 mM; the reaction mixtures were incubated at 25^{o}C for 10 min, and the absorbance was measured at room temperature.

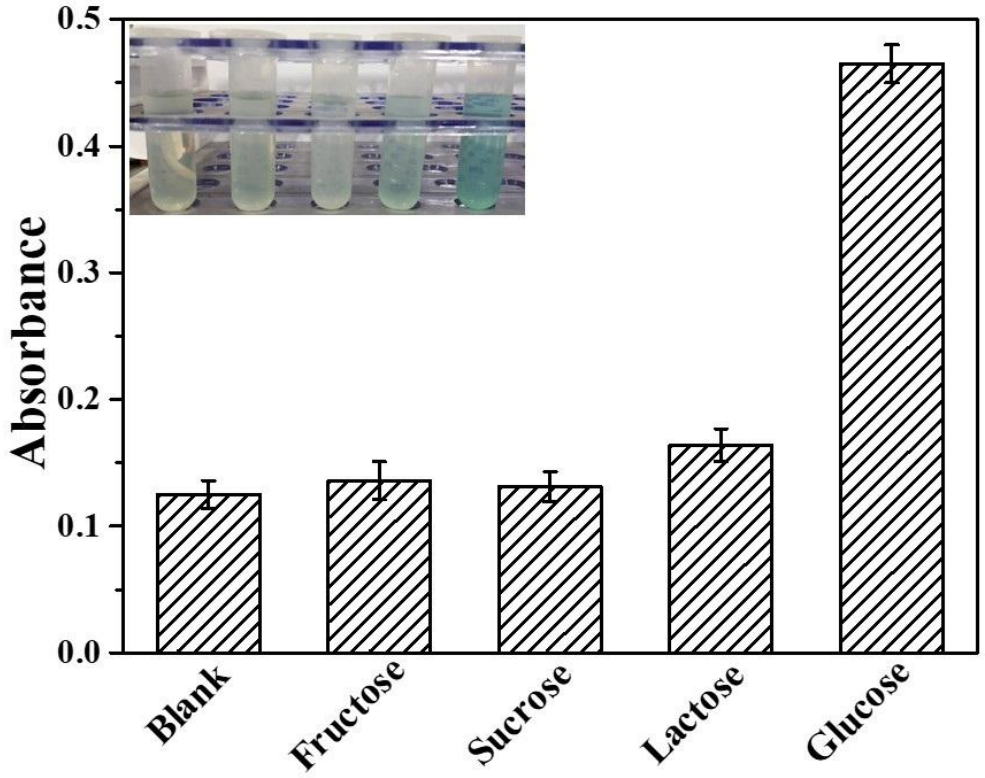

Figure 11. The selectivity of glucose detection with 5 mM fructose, 5 mM sucrose, 5 mM lactose, and 0.5 mM glucose after incubation with glucose oxidase and $20CeO_2$/Y nanocomposite catalysts. Experimental conditions: catalysts: 0.2 mg; acetate buffer: 0.2 M (pH=3.6); PBS buffer (pH 7.0); TMB, 8 mM; the reaction mixtures were incubated at 25^{o}C for 10 min, and the absorbance was measured at room temperature.

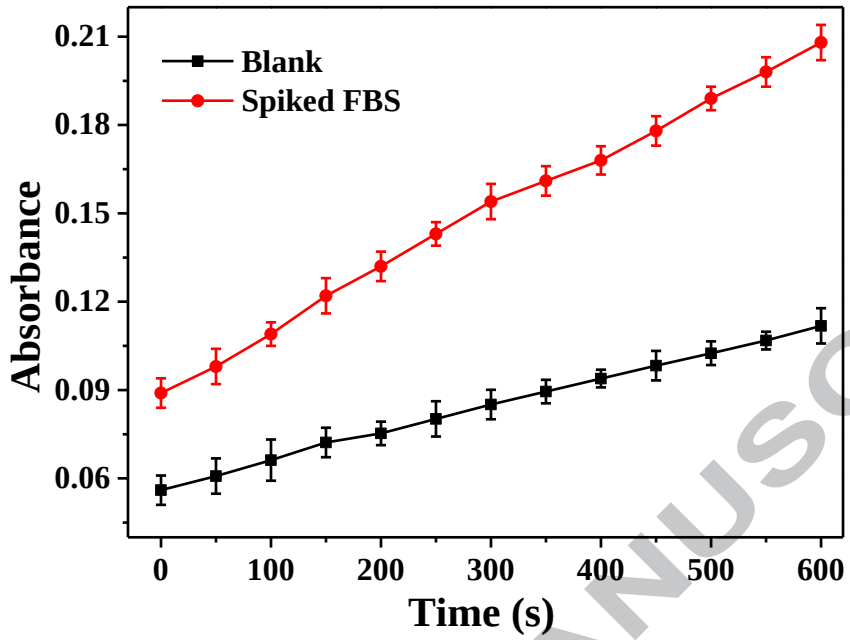

Figure 12. Time dependent absorbance changes at 652 nm for blank and spiked FBS samples after incubation with glucose oxidase and $20CeO_2/Y$ nanocomposite catalysts. Experimental conditions: catalysts: 0.2 mg; acetate buffer: 0.2 M (pH=3.6); PBS buffer (pH 7.0); TMB, 8 mM; spiked FBS: 5 mM; the reaction mixtures were incubated at 25^{o}C for 10 min, and the absorbance was measured at room temperature.

Table 1. Comparison of the apparent Michaelis−Menten constant (K_m), the maximum reaction rate (V_m) and the catalytic constant (k_{cat}) obtained from the double reciprocal plots

Substrate	Catalyst	K_m (mM)	V_{max} (mM· min^{-1})	k_{cat} (min^{-1})
TMB	$20CeO_2/Y$	1.52	0.25	0.164
TMB	HRP[#]	5.90	0.11	0.019
H_2O_2	$20CeO_2/Y$	0.15	7.74	51.6
H_2O_2	HRP[#]	0.63	1.35	2.14

[#] The values of K_m and V_{max} for HRP are from the literature [48].

Rational Design of a Stable Peroxidase Mimic for Colorimetric Detection of H_2O_2 and Glucose: A Synergistic CeO_2/Zeolite Y Nanocomposite

Xiaowei Cheng, Le Huang, Xuanyu Yang, Ahmed A. Elzatahry, Abdulaziz Alghamdi, and Yonghui Deng

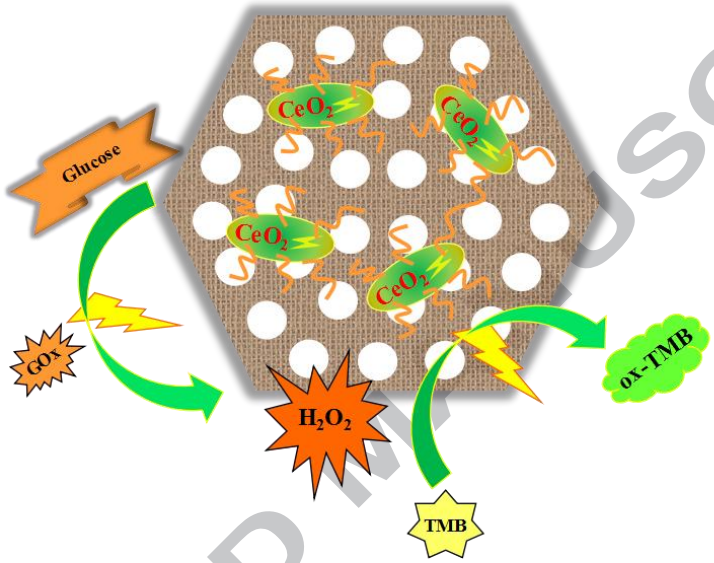

A facile colorimetric assay was developed for the accurate detection of H_2O_2 and glucose with the CeO_2/Y hybrid nanocomposite as a highly efficient peroxidase-mimicking nanozyme, which shows the synergistic effects of outstanding activity of highly dispersed CeO_2 nanoparticles and high surface area and pore volume of zeolite Y as support.